

NON LINEAR ANALYSIS OF REINFORCED CONCRETE BEAMS BY THE B₃ SPLINES FINITE STRIP METHOD

João Gilberto Teixeira Silva, Doutorando, jgts@click21.com.br

José Inácio de Souza Leão Ávila, PhD, jisla@ufpe.br

Departamento de Engenharia Civil, Universidade Federal de Pernambuco.

Av. Acad. Hélio Ramos, Cidade Universitária – Recife – PE – Brasil.

Abstract. A B₃ Spline Finite Strip Method (SFSM) approach for the analysis of reinforced concrete beam is presented. The structure is modeled as a group of longitudinal strips which are divided in number of sections. In this direction, the displacements are interpolated by B₃ Splines functions (cubic interpolation) and in the transversal direction the displacements are interpolated by quadratic Lagrangian polynomial function.

The analysis can be either linear or non linear. In the first, elastic and linear behavior is considered, in the second, the non linearity is accounted for concrete cracking, bond slip effects, and yielding of the steel. The Finite Element Method (FEM) is a powerful numerical tool to deal with both types of analyzes any kind of structures as well as with different support condition and geometry of the structure. However, it requires large amount of unknowns and, as a consequence, a high computational cost.

Cheung (1968) developed a numeric formulation which used a computational treatment similar to the FEM with the advantage of having a cheaper computational cost. This formulation is the base of Finite Strips B₃ Splines method.

In this paper two examples are analyzed and comparisons of the results from the proposed formulation, either taking into account perfect adherence, with the experimental load-displacement curve are carried out.

The comparisons have shown that the Finite Strips B₃ Splines method get accurate results.

Keywords: spline functions, finite strip method, concrete, plasticity.

1. REVIEW

Cheung & Cheung (1973) developed a study about the analysis of curved bridge beams and with cellular section using for this purpose the FSM with harmonic functions. These authors used a system of polar coordinates to the beam section flanges and system of cylindrical coordinates to the beam section webs. Two examples were analyzed.

Cheng *et al* (1987) developed a study about static and dynamic rectangular plate analysis as well as about the plate stability. These plates were stiffened in the x and y directions. B₃ Splines interpolation function were used to describe the displacements in both directions (x and y directions).

Ávila (1988) presented a study about plates and cellular curved beams using B₃ Splines functions with unequal intervals. Curvature compatibility along nodal lines were assumed by using a fifth order polynomial function and an auxiliary nodal line located in mid-width of the strip.

Sheikh & Mukhopadhyay (1992) analyzed plates with several boundary conditions, loadings and shapes as well as with stiffeners localized in any direction.

Hinton & Rao (1993) employed the semi-analytical finite strip method to optimize the shape of the shells and cellular structures minimizing the strain energy and keeping the material volume constant.

Cheung & Au (1994) developed a study of shells where was employed isoparametric formulation with B₃ Splines in mapping of the domain of the structure and in the displacements interpolation. Several examples were analyzed and the results compared with the analytical results.

Ng & Chen (1995) developed a study about arbitrary planform of plates by a mapping technique with cubic polynomials. Wang & Li (2000) analyzed lateral buckling of thin walled structures in which B₃ spline functions were employed to perform the interpolation of the displacements due to lateral buckling. This analysis considered the shear strain effect on the middle surface of the wall. Three examples were analyzed and the results were compared with the results of classical theory and others methods. The comparisons showed the versatility, precision and the efficiency of the method.

Eccher *et. al* (2005) published a study about analysis of plates in plane stresses and with any geometry openings. The authors employed an isoparametric formulation and a numerical technique that divided the strips around openings in sub-strips.

2. THE FINITE STRIP METHOD WITH B₃ SPLINES.

The Finite Element Method (FEM) is regarded as the most powerful method of structural analysis and is theoretically applicable to any structure. However for a number of applications, it is expensive due to the demands for large computer and data preparation. The semi-analytical Finite Strip Method (FSM) with harmonic series is more economical but implicitly imposes the conditions that the structure has to be simply supported at the ends and is not usable for geometry variations.

The Spline Finite Strip Method (SFSM), which has similarities with both FEM and FSM, overcomes these difficulties combining the versatility of the former in dealing with different support conditions with the simplicity of the latter in the input of data.

In this work, the B3-Spline functions with equal intervals are used to describe the longitudinal variations of the displacement whereas the transverse shape is described by lower order polynomials.

2.1 Cubic spline functions.

The B3-Cubic Spline interpolating functions are composed by the association of third degree polynomials with validity range restricted to four previously fixed intervals. The general form is written as

$$\Phi(x) = \sum_{i=1}^{m+1} \alpha_i \varphi_i(x) \tag{1}$$

where α_i are the spline point parameters and the unknowns of the method, m is the number of intervals that the strip is divided into and $\varphi_i(x)$ are the local splines defined by

$$\varphi(x) = \frac{1}{6b^3} \begin{cases} (x-x_{i-2})^3 & x_{i-2} \leq x \leq x_{i-1} \\ b^3 + 3b^2(x-x_{i-1}) + 3b(x-x_{i-1})^2 - 3(x-x_{i-1})^3 & x_{i-1} \leq x \leq x_i \\ b^3 + 3b^2(x_{i+1}-x) + 3b(x_{i+1}-x)^2 - 3(x_{i+1}-x)^3 & x_i \leq x \leq x_{i+1} \\ (x_{i+2}-x)^3 & x_{i+1} \leq x \leq x_{i+2} \end{cases} \tag{2}$$

The profile of function $\varphi_i(x)$ can be seen in Fig.1, where x varies in the interval (x_0, x_m) and $b = \frac{(x_m - x_0)}{m}$. Figure 2 shows a graphic of the assembled splines.

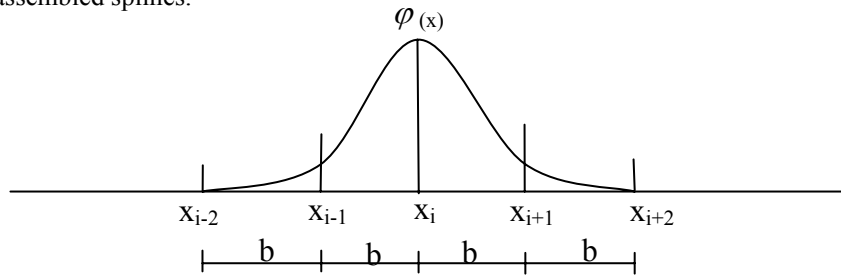


Figure 1. Cubic spline curve.

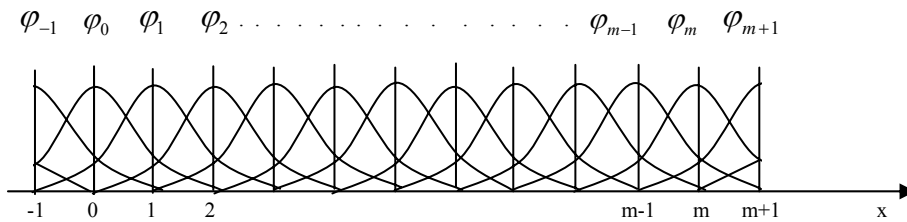


Figure 2. Family of cubic polynomial curves.

2.2 Displacement functions

In the FSM, similarly to FEM, the displacement (u) in a fixed direction can be expressed by the product of two independent shape functions, that is:

$$u(x, y) = \sum_{i=1}^{m+1} \sum_{k=1}^3 L(y)_k \varphi(x)_i^k \alpha_i^k = \{L\} \{\varphi\} \{\alpha\} \tag{3}$$

where $\{\varphi(x)\} = \{\varphi(x)_{-1}\varphi(x)_0\varphi(x)_1\dots\varphi(x)_{m+1}\}$ is the interpolation function vector and $\{\alpha\} = \{\alpha_{-1}\alpha_0\alpha_1\dots\alpha_{m+1}\}^T$ is the generalized displacement vector. The vector $\{\alpha\} = \{\alpha_{-1}\alpha_0\alpha_1\dots\alpha_{m+1}\}^T$ is composed by auxiliary parameter and, physically, do not represents the real displacements field. The functions $L(y)$ are lower order polynomials of quadratic variation and are written as

$$\begin{aligned} L_1 &= 1 - \frac{3y}{a} + 2\frac{y^2}{a^2} \\ L_2 &= \frac{4y}{a} - \frac{4y^2}{a^2} \\ L_3 &= -\frac{y}{a} + \frac{2y^2}{a^2} \end{aligned} \tag{4a-c}$$

The spline functions, presented in Eq.3, represent the variations of the displacement in the x directions, as shown in Fig. 3. In this work, they are associated to the longitudinal direction along the span of the beam. On the other hand, the functions $L(y)$ were adopted for describing the variations in the transverse direction.

2.1 Spline elements discretization.

The mesh is obtained by dividing the structure into a number of longitudinal strips parallel to x direction and defined by two nodal lines $j=1$ e $j=3$, as shown in Fig 3. An auxiliary nodal line ($j=2$) located at mid width $a/2$ is required in order to use a 2nd order polynomial. The length a is the width of a generic strip.

Each strip is divided in m spline segments defined by $m+1$ spline knots in the y direction equally spaced with a length equal to b . The procedure also requires two fictitious knots at the ends of the strips, away from the extremities of the a distance L/m .

Therefore, by means of Eq. (1), (2) and (3) the displacement field in a generic point is described by

$$\begin{Bmatrix} u \\ v \end{Bmatrix} = \begin{bmatrix} L1 & 0 & L2 & 0 & L3 & 0 \\ 0 & L1 & 0 & L2 & 0 & L3 \end{bmatrix} \begin{Bmatrix} u1 \\ v1 \\ u2 \\ v2 \\ u3 \\ v3 \end{Bmatrix} = \begin{bmatrix} [L1] & [L2] & [L3] \end{bmatrix} \begin{Bmatrix} \{U1\} \\ \{U2\} \\ \{U3\} \end{Bmatrix} \tag{5}$$

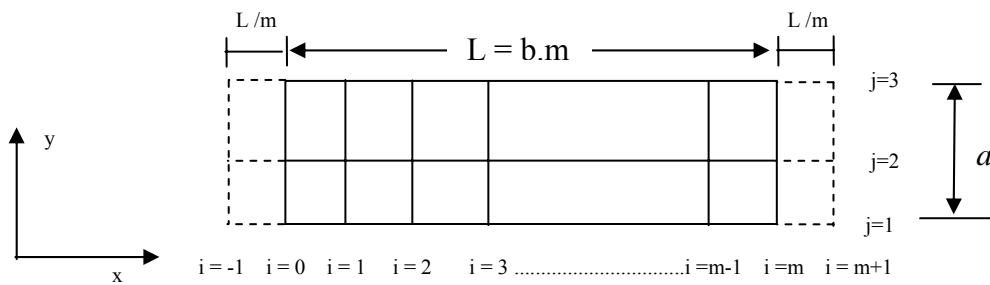


Figure 3. Detail of a strip.

2.3. Strain and stress/spline parameter relationships for plane stresses.

The in-plane strains are related to the longitudinal and transverse displacement by the following equations

$$\{\varepsilon\} = \begin{Bmatrix} \varepsilon_x \\ \varepsilon_y \\ \gamma_{xy} \end{Bmatrix} = \begin{Bmatrix} \frac{\partial u}{\partial x} \\ \frac{\partial v}{\partial y} \\ \frac{\partial u}{\partial y} + \frac{\partial v}{\partial x} \end{Bmatrix} \quad (6)$$

Thus, using equations 1, 2 and 5, the equation 6 can be re-written in function of the spline parameters as:

$$\{\varepsilon\} = \begin{bmatrix} [B]_{i-2} & [B]_{i-1} & [B]_i & [B]_{i+1} \end{bmatrix} \begin{Bmatrix} \{\alpha\}_{i-2} \\ \{\alpha\}_{i-1} \\ \{\alpha\}_i \\ \{\alpha\}_{i+1} \end{Bmatrix} = [B]\{\alpha\} \quad (7)$$

where $[B]_{j=i-2, i-1, i, i+1}$ are composed by the derivatives of the shape functions.

Accordingly, the stresses can also be obtained by:

$$\{\sigma\} = [E] \begin{bmatrix} [B]_{i-2} & [B]_{i-1} & [B]_i & [B]_{i+1} \end{bmatrix} \begin{Bmatrix} \{\alpha\}_{i-2} \\ \{\alpha\}_{i-1} \\ \{\alpha\}_i \\ \{\alpha\}_{i+1} \end{Bmatrix} = [E][B]\{\alpha\} \quad (8)$$

in which $[E]$ is the matrix of the physical properties of the material.

2.4 Stiffness Matrix Formulation

The minimization procedure of total potential energy of the structure yields the following system of equation:

$$[K]\{\alpha\} = \{P\} \quad (9)$$

where $[K]$ is the overall stiffness matrix, $\{\alpha\}$ is the vector of the parameters and $\{P\}$ is the overall force matrix.

The stiffness matrix is symmetrical, banded and composed by adding the stiffness matrix of the individual segments of the strips which can be written as:

$$[K] = \int_0^a \int_0^L [B]^T [E][B] |J| dx dy \quad (10)$$

where $[B]$ is the matrix which relates the strains and the spline displacements, $[E]$ is the matrix which relates the stress and the strains and $|J|$ is the jacobian matrix determinant.

The strip stiffness matrix is easily formed since it is enough to determine only the stiffness matrix of a spline segment due to the equally spaced knot. The assembling follows the degrees of freedom numbering, similarly to the FEM. More detail can be found in Avila (1988).

3. NON LINEAR ANALYSIS FORMULATION

3.1 Introduction

Reinforced concrete structures are made up of two materials, concrete and steel. Steel is a homogeneous material and its material properties are generally well defined. Concrete is, however, a heterogeneous material made up of

cement, mortar and aggregates. Its mechanical properties scatter more widely and cannot be defined easily (Kwak & Filippou (1990)).

The nonlinear concrete response is caused by two major effects, cracking of concrete in tension, and yielding of the reinforcement or crushing of concrete in compression.

In present study, the stiffness of concrete and reinforcing steel are formulated separately, the results are then superimposed to obtain the element stiffness. Is adopted the smeared crack model in the description of the behavior of cracked concrete, and cracking in more than one direction is represented by a system of orthogonal cracks and the crack direction changes with load history.

The reinforcing steel is assumed to carry stress along its axis only and the effect of dowel action of reinforcement is neglected and is admitted perfect bond between rebar and the surround concrete.

3.2 Behavior of concrete

According Kwak & Filippou (1990) the concrete stress-strain relation exhibits nearly linear elastic response up to about 30% of the compressive strength. This is followed by gradual softening up to the concrete compressive strength, when the material stiffness drops to zero. Beyond the compressive strength the concrete stress-strain relation exhibits strain softening until failure takes place by crushing.

In present study is adopted the orthotropic model due to its simplicity. According Kwak & Filippou (1990) “It can match rather well experimental data under proportional biaxial loading and approximates the concrete behavior under general biaxial loading adequately”. It is particularly suitable for the analysis of structures under stress state predominantly biaxial, like reinforced concrete beams, panels and shells.

Under combinations of biaxial compressive stress concrete exhibits strength and stress-strain behavior which is different from that under uniaxial loading conditions. Figure 4 shows the biaxial strength envelope of concrete (Kupfer's failure envelope) under proportional loading. Under a combination of tension and compression, the compressive strength decreases almost linearly with increasing principal tensile stress and under biaxial tension concrete exhibits constant or perhaps slightly increased tensile strength compared with that under uniaxial loading

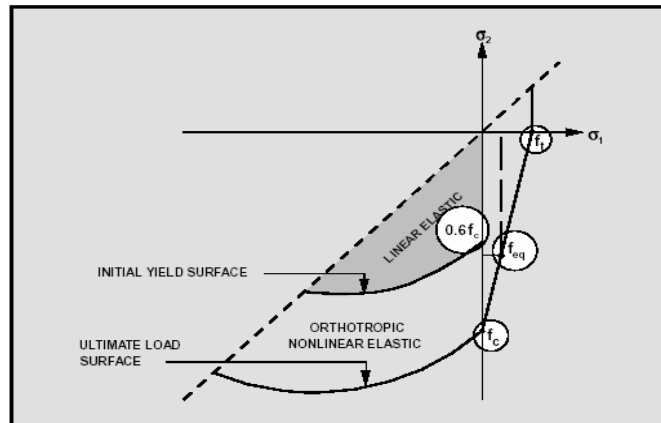


Figure 4. Strength failure envelope of concrete -Kwak & Filippou (1990)

In the biaxial compression region (Figure 4) the model is linear elastic for stress combinations inside the initial yield surface. When stress combinations are outside the initial yield surface but inside the ultimate failure surface the behavior of concrete is described by a nonlinear orthotropic model. For biaxial stresses outside the Kupfer's failure envelope, concrete enters into the strain softening range of behavior where an orthotropic model describes the biaxial behavior. If the principal compressive strain exceeds the limit value ϵ_{iu} (see fig 5), the failure in this region occurs by crushing of concrete.

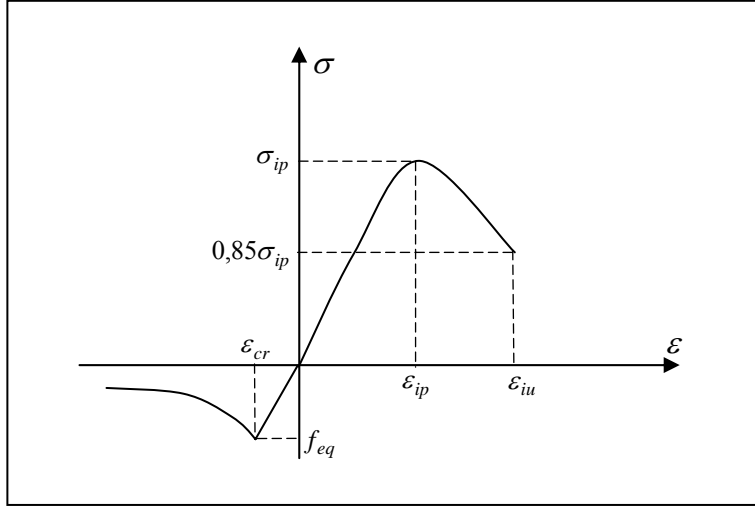


Figure 5. Stress-strain relation of concrete

The parameters of the equivalent uniaxial stress-strain relationship, shown in Figure 5, in the main axes of orthotropy can now be summarized for the compression-compression region of the principal stress space as following

$$\alpha = \frac{\sigma_1}{\sigma_2} \quad (11)$$

$$\sigma_{2p} = \frac{1 + 3,65\alpha}{(1 + \alpha)^2} \cdot f_c \quad (12)$$

$$\varepsilon_{2p} = \varepsilon_c \left(\frac{3\sigma_2}{f_c} - 2 \right) \quad (13)$$

$$\sigma_{1p} = \alpha \sigma_{2p} \quad (14)$$

$$\varepsilon_{1p} = \varepsilon_c \left[-1,6 \left(\frac{\sigma_{1p}}{f_c} \right)^3 + 2,25 \left(\frac{\sigma_{1p}}{f_c} \right)^2 + 0,35 \left(\frac{\sigma_{1p}}{f_c} \right) \right] \quad (15)$$

$$\sigma_i = -\sigma_{ip} \left[2 \frac{\varepsilon_i}{\varepsilon_{ip}} - \left(\frac{\varepsilon_i}{\varepsilon_{ip}} \right)^2 \right] \quad (16)$$

where f_c is the uniaxial compressive strength, ε_c is the uniaxial compressive strain and $i=1,2$ defines the orthotropic axes.

In the compression-tension or tension-tension regions the principal stress can written as following

$$\sigma_i = E_c \varepsilon \quad \text{if } \varepsilon \leq \varepsilon_{cr} \quad (17)$$

where $\varepsilon_{cr} = 0,33\sqrt{f_c(MPa)}/E_c$, and E_c is the initial elastic modulus of concrete. After cracking, concrete tension-stiffening effects are significant and must be included. The constitutive relations used in present study is that proposed by Vecchio (1990)

$$\sigma_i = \frac{f_{eq}}{1 + \sqrt{200\varepsilon}} \quad \text{if } \varepsilon > \varepsilon_{cr} \quad (18)$$

For the later regions the following assumptions are adopted in this study: (1) failure takes place by cracking and, therefore, the tensile behavior of concrete dominates the response; (2) the uniaxial tensile strength of concrete is reduced to the value f_{eq} , as shown in Figs. 4 and 5 to account for the effect of the compressive stress; in the tension-tension region the tensile strength remains equal to the uniaxial tensile strength f_t (Figure 4); (3) the concrete stress-strain relation in compression is the same as under uniaxial loading and does not change with increasing principal tensile stress. Thus $\sigma_{ip} = f_c$ in Figure 5 and ε_{iu} is equal to uniaxial crushing strain ε_{cu} .

3.3 Concrete Material Matrix

For stress combinations inside the initial yield surface in Figure 2.2 concrete is assumed to be a homogeneous, linear isotropic material. Thus, the stress-strain relation for plane stress problems has the simple form

$$\begin{Bmatrix} \sigma_x \\ \sigma_y \\ \tau_{xy} \end{Bmatrix} = \frac{E_c}{1-\nu^2} \begin{bmatrix} 1 & \nu & 0 \\ \nu & 1 & 0 \\ 0 & 0 & 0,5(1-\nu) \end{bmatrix} \quad (19)$$

where E_c is the initial elastic modulus and ν is Poisson's ratio.

Once the biaxial stress combination exceeds the initial yield surface in the compression-compression region concrete is assumed to behave as an orthotropic material.

With reference to the principal axes of orthotropy the incremental constitutive relationship can be expressed by

$$\begin{Bmatrix} d\sigma_{11} \\ d\sigma_{22} \\ d\tau_{12} \end{Bmatrix} = \frac{1}{(1-\nu^2)} \begin{bmatrix} E_{c1} & \nu\sqrt{E_{c1}E_{c2}} & 0 \\ \nu\sqrt{E_{c1}E_{c2}} & E_{c2} & 0 \\ 0 & 0 & (1-\nu^2)G \end{bmatrix} \begin{Bmatrix} d\varepsilon_{11} \\ d\varepsilon_{22} \\ d\gamma_{12} \end{Bmatrix} = [E_c] \begin{Bmatrix} d\varepsilon_{11} \\ d\varepsilon_{22} \\ d\gamma_{12} \end{Bmatrix} \quad (20)$$

where E_{c1} and E_{c2} are the secant moduli of elasticity in the direction of the axes of orthotropy, which are oriented perpendicular and parallel to the crack direction and $(1-\nu^2)G = 0,25(E_{c1} + E_{c2} - 2\nu\sqrt{E_{c1}E_{c2}})$.

If any of the principal strains exceeds the concrete cracking strain (ε_{cr}), then the concrete is assumed to have cracked and the Poisson's ratio is taken as zero in Eq. 20.

The material matrix is defined with reference to principal strain direction, it must be transformed to the global coordinate system before all element stiffness matrices can be assembled, thus

$$[E]_{GL} = [T_c]^T [E_c] [T_c] \quad (21)$$

where $[T_c]$ the concrete transformation matrix

3.4 Behavior of Reinforcing Steel

The specification of a single stress-strain relationship is sufficient to define the material properties needed in the analysis of reinforced concrete structures. This relation exhibits an initial linear elastic portion and a yield plateau as can be seen in Figure 6.

The equivalent steel element has uniaxial properties in the direction parallel to the axis of the reinforcing bars. The constitutive material model takes the simple form

$$\begin{Bmatrix} \sigma_1 \\ \sigma_2 \\ \tau_{12} \end{Bmatrix} = \begin{bmatrix} E_{s1} & 0 & 0 \\ 0 & 0 & 0 \\ 0 & 0 & 0 \end{bmatrix} \begin{Bmatrix} \varepsilon_1 \\ \varepsilon_2 \\ \gamma_{12} \end{Bmatrix} = [E_s] \begin{Bmatrix} \varepsilon_1 \\ \varepsilon_2 \\ \gamma_{12} \end{Bmatrix} \quad (22)$$

where $E_{s,j}$ is Young's modulus of reinforcing steel (see figure 6).

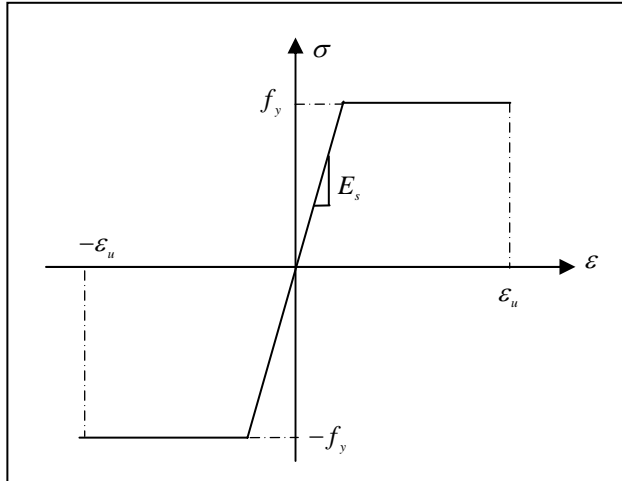


Figure 6. Steel stress-strain relation

According to Figure 7 when the angle θ takes a value different from zero, the local stiffness matrix in Eq. 22 needs to be transformed to the global xy coordinate system before it can be assembled into the structure stiffness matrix, thus

$$[E_s]_{GL} = [T_s]^T [E_s] [T_s] \quad (23)$$

where $[T_s]$ is the steel transformation matrix

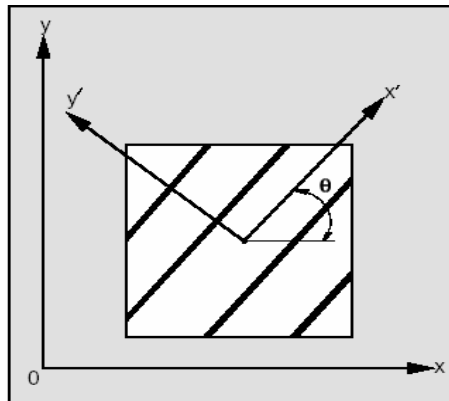


Figure 7. Coordinate transformation for steel

4. APPLICATIONS OF THE PROPOSED FORMULATION.

4.1 Details of the models.

The proposed formulation was used to analyze two different structures obtained in the technical literature. These structures were simple supported beams previously studied by Kwak and Fillipou (1990). In their work, the authors presented the experimental results of the beams submitted to a concentrated load at mid-span up to failure.

The span length, in both beams, was equal to 3,66m, as shown in Fig. 8 and their mechanical properties are given in table 1.

The cross-sectional dimensions and the geometric percentage of reinforcement were different for each beam. In the beam in Case 1, the amount of longitudinal reinforcement was about 1,36% of the cross-section and, in Case 2, it was lower and around 1,0%. However, in the later, there was compressive reinforcement as well transverse reinforcement formed by vertical stirrups. Table 2 presents geometric details of both beams.

Table 1 – Mechanical properties for the beam materials, in MPa.

CASE	f_c	E_c	f_s	E_s
1	33,28	26000,00	315,00	200000,00
2	24,10	23200,00	556,00	218000,00

Table 2 – Geometric details of the beams.

CASE	h (m)	w (m)	As_l (cm ²)	As_l' (cm ²)	As_w (cm ² /m)
1	0,51	0,20	14,0	-	-
2	0,553	0,305	16,0	2,0	4,9

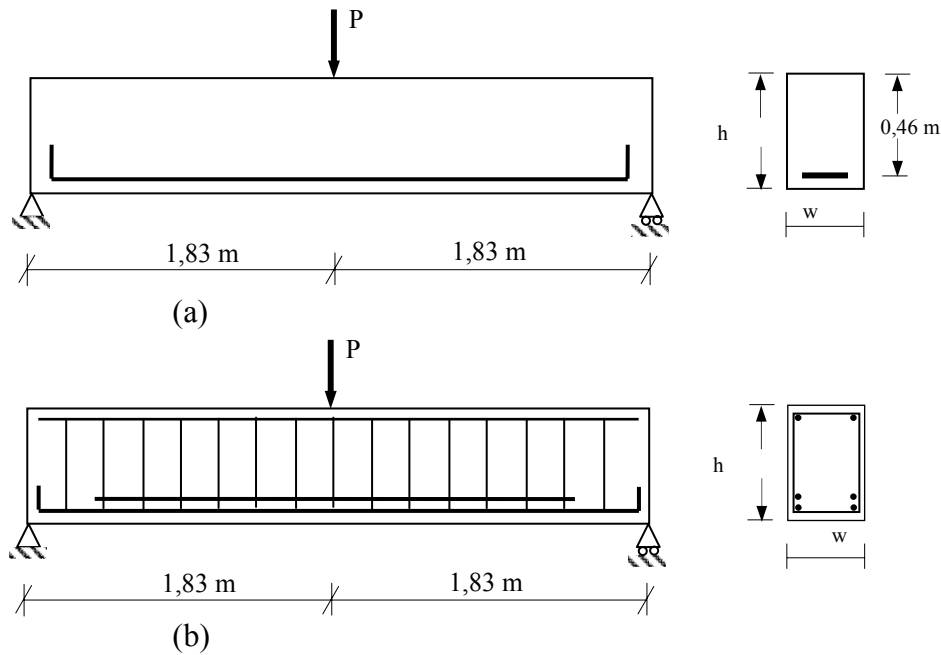


Figure 8. Beam geometry and reinforcements: (a) Case 1 (b) case (2)

The simulations of the beam behavior were carried out using only half of the length due to the loading and geometrical symmetry. The mesh of both model, shown in figure 9, also maintained similarities, that is, both were formed by one longitudinal strip divided into five equally spaced spline knots.

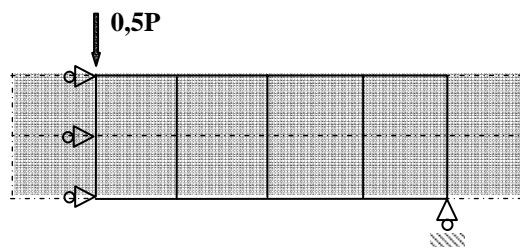


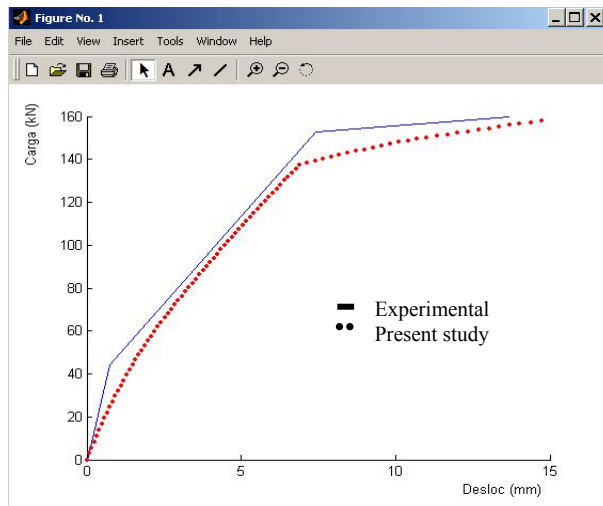
Figure 9. Mash adopted to both cases

4.1 Analysis of the results.

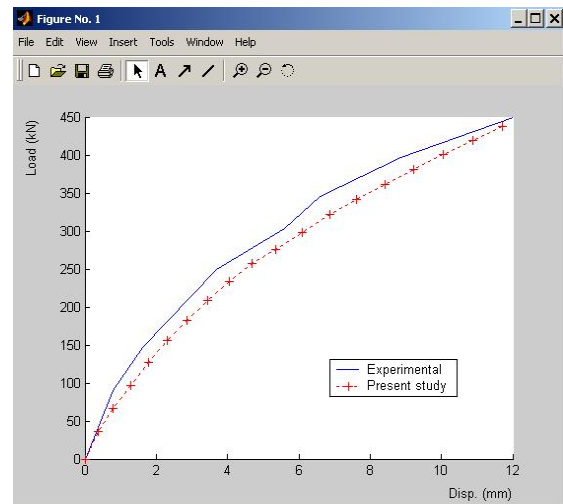
The experimental and theoretical results obtained with the proposed method are shown in figure 10, for Case 1 and Case 2.

As can be seen, in Case 1, the experimental graphic presents a discontinuity near the failure load. On the other hand, the graphic formed by the theoretical results presents two distinct discontinuities: one near a load of 45 kN and the other close to failure load. In Case 2, the beam presents a fragile behavior differently from the beam of Case 1 without shown any discontinuity. It can be noted that, like the experimental graphic, the graphic of the proposed method also do not presents discontinuity.

The proposed method seems to simulate a stiffer structure since it produces higher loads for a fixed displacement. However, the differences are quite small. In spite of the detached differences, it can be seen that the graphics in both cases are very close between them and produce results with good accuracy even with the coarse mesh adopted.



(a)



(b)

Figure 10. Load-displacement curves: (a) Case 1 (b) Case 2

5. CONCLUSIONS

A new approach for the Spline Finite Strip Method has been successfully developed. The studied cases have showed that the theoretical load-displacement curves produced by the proposed formulation describe precisely the experimental load-displacement curve as well as the load failure. The smallest amount of degree of freedom possible was used in the examples.

6. ACKNOWLEDGMENTS

The authors thank the FAPEAL by the sponsoring of the first author and also all member of the Department of Civil Engineering of the Federal University of Pernambuco (UFPE) by the direct and undirect aid to development of this work.

7. REFERENCES

- Ávila, J. I. S. L.; 1988, "Curved concrete bridge of segmental box construction with inclined webs". PhD thesis, University of Leeds, Department of Civil Engineering. February
- Cheng, Y. K.; Au, F. T. K.; 1994, "Isoparametric spline finite strip for degenerate shells". *Thin -Walled Structures*, vol. 21, pp. 65 – 92.
- Cheng, S. P.; Dade, H.; Zongmu, W.; 1987, "Static, vibration and stability analysis of stiffened plates using B_3 splines functions". *Computers & Structures*, vol. 27, No. 1, pp. 73 – 78.
- Cheung, M. S.; Cheung, Y. K.; 1973, "Analysis of curved box girder bridges by finite strip method". *IABSE Publications*, vol. 31, pp. 1 – 19.
- Eccher, G; Rasmussen, K. J. R; Baldassino, N; Zandonine, R.; 2005, "Isoparametric spline finite strip method for in plane stress analysis". University of Sidney, Centre
- Hinton, E.; Rao, N. V. R.; 1993, "Structural shape optimization of shells and folded plates using two noded finite strips". *Computer & Structures*, Vol. 46, No. 6, pp. 1055 – 1071.
- Kwak, H. G.; Fillippou, F. C.; 1990, "Finite element analysis of reinforced concrete structures under monotonic loads", University of California, Department of Civil Engineering.
- Ng, S. F.; Chen, X.; 1995, "Analysis of arbitrary Mindlin plates of bridge decks by spline finite strip method", *Computer & Structures*, Vol 54, pp 111- 118.
- Polak, M. A.; Vecchio, F. J.; 1993, "Nonlinear analysis of reinforced-concrete shells". *Journal of Structural Engineering*, vol. 119, No 12, pp. 3439 – 3459.
- Sheikh, A. H.; Mukhopadhyay, M.; 1992, "Analysis of stiffened plate with arbitrary planform by the general spline finite strip method", *Computer & Structures*, Vol. 42, No. 1, pp. 53 – 67.
- Vecchio, F. J.; Collins, M. P.; 1986, "The modified compression - field theory for reinforced concrete elements subjected to shear". *ACI Structural Journal*, March - April, pp. 219 - 231.

- Vecchio, F. J.; 1990, "Reinforced concrete membrane element formulations". Journal of Structural Engineering, vol. 116, pp. 730 - 750.
- Wang, Q; Li, W. Y.; 2000, "Lateral buckling of thin-walled member with shear lag using Spline finite member element method". Computer & Structures, pp 81-91.

8. RESPONSIBILITY NOTICE

The authors are the only responsible for the printed material included in this paper.